JOURNAL OF COMPUTATIONAL PHYSICS 8, 230–240 (1971)

Numerical Method for Almost Three-Dimensional Incompressible Fluid Flow and a Simple Internal Obstacle Treatment*

P. I. NAKAYAMA AND N. C. ROMERO

University of California, Los Alamos Scientific Laboratory, Los Alamos, New Mexico 87544

Received January 5, 1971

An extension of the Simplified Marker and Cell (SMAC) method for the numerical solution of incompressible flows is used to investigate transient flows that are almost three dimensional. The equations of motion are two dimensional but contain functions that account for the effects of a third dimension. The method that results from this extension may also be used for the simple incorporation of internal obstacles in two-dimensional flows.

INTRODUCTION

There is a class of incompressible fluid flow problems which, while having important three-dimensional effects, are nevertheless "almost" two-dimensional. Examples include flows between slowly contracting or dilating parallel rigid surfaces, such as might occur in an extrusion process, and flows over a smoothly sculptured terrain. Although these examples may be studied by a full three-dimensional numerical program such as the Simplified Marker and Cell (SMAC) [1] method, such calculations are extremely time consuming and require the largest computers now available. Alternatively, if the distance between the bounding surfaces is changing slowly with position, as for example in Fig. 3, then considerable simplification can be realized by the use of the approximate equations derived below.

The equations are two dimensional, but contain functions that account for the effects of the third dimension. These functions may also be used to easily describe internal rigid obstacles in real two-dimensional flows.

The equations of motion are solved numerically using a SMAC-like method and are illustrated with two calculational examples.

* This work was performed under the auspices of the United States Atomic Energy Commission.

Differential Equations, Constant Wall Configuration

The starting point is the set of conservative equations for the velocity components, u, v, and w, in the x, y, and z directions, respectively:

$$\frac{\partial u}{\partial x} + \frac{\partial v}{\partial y} + \frac{\partial w}{\partial z} = 0, \tag{1}$$

$$\frac{\partial u}{\partial t} + \frac{\partial u^2}{\partial x} + \frac{\partial uv}{\partial y} + \frac{\partial uw}{\partial z} = -\frac{\partial \phi}{\partial x} + \nu \nabla^2 u, \tag{2}$$

$$\frac{\partial v}{\partial t} + \frac{\partial uv}{\partial x} + \frac{\partial v^2}{\partial y} + \frac{\partial vw}{\partial z} = -\frac{\partial \phi}{\partial y} + \nu \nabla^2 v, \tag{3}$$

$$\frac{\partial w}{\partial t} + \frac{\partial uw}{\partial x} + \frac{\partial vw}{\partial y} + \frac{\partial w^2}{\partial z} = -\frac{\partial \phi}{\partial z} + \nu \nabla^2 w. \tag{4}$$

The ratio of pressure to constant density is ϕ, while ν is the constant coefficient of kinematic-viscosity.

The flow is bounded by surfaces that lie at $z = a(x, y)$ and $z = b(x, y)$, with $a < b$. At these surfaces, the boundary conditions are

$$\left.\begin{aligned} w &= u\frac{\partial a}{\partial x} + v\frac{\partial a}{\partial y} \\ w &= u\frac{\partial b}{\partial x} + v\frac{\partial b}{\partial y} \end{aligned}\right\} \quad \begin{aligned} &\text{at} \quad z = a, \\ &\text{at} \quad z = b. \end{aligned} \tag{5}$$

Equations (1)–(4) are to be integrated from $z = a$ to $z = b$. For example, Eq. (1) then becomes

$$\int_a^b \left(\frac{\partial u}{\partial x} + \frac{\partial v}{\partial y}\right) dz + w(b) - w(a) = 0.$$

Using Eq. (5), we can obtain

$$\int_a^b \left(\frac{\partial u}{\partial x} + \frac{\partial v}{\partial y}\right) dz + u(b)\frac{\partial b}{\partial x} + v(b)\frac{\partial b}{\partial y} - u(a)\frac{\partial a}{\partial x} - v(a)\frac{\partial a}{\partial y} = 0.$$

According to Leibnitz' rule, this can be transformed to

$$\frac{\partial}{\partial x}\int_a^b u\, dz + \frac{\partial}{\partial y}\int_a^b v\, dz = 0. \tag{6}$$

In the same way, Eqs. (2) and (3) also can be transformed to eliminate the explicit dependence upon vertical velocity, w:

$$\frac{\partial}{\partial t}\int_a^b u\,dz + \frac{\partial}{\partial x}\int_a^b u^2\,dz + \frac{\partial}{\partial y}\int_a^b uv\,dz$$

$$= -\int_a^b \frac{\partial \phi}{\partial x}\,dz + \nu\int_a^b \left(\frac{\partial^2 u}{\partial x^2} + \frac{\partial^2 u}{\partial y^2}\right) dz + \nu\left[\left(\frac{\partial u}{\partial z}\right)_{z=b} - \left(\frac{\partial u}{\partial z}\right)_{z=a}\right], \tag{7}$$

$$\frac{\partial}{\partial t}\int_a^b v\,dz + \frac{\partial}{\partial x}\int_a^b uv\,dz + \frac{\partial}{\partial y}\int_a^b v^2\,dz$$

$$= -\int_a^b \frac{\partial \phi}{\partial y}\,dz + \nu\int_a^b \left(\frac{\partial^2 v}{\partial x^2} + \frac{\partial^2 v}{\partial y^2}\right) dz + \nu\left[\left(\frac{\partial v}{\partial z}\right)_{z=b} - \left(\frac{\partial v}{\partial z}\right)_{z=a}\right]. \tag{8}$$

Equation (4) could also be similarly transformed, but we shall replace it by some assumptions regarding the variations of the field variables with z, and accordingly no longer require it for the derivations.

Equations (6)–(8) incorporate no assumptions; they are rigorous consequences of the starting equations. Our procedure for making them complete is to assume a specific form for the variation of u and v with z. With the bounding surfaces at rest, it would be appropriate to make the approximations

$$\left.\begin{aligned} u(x, y, z, t) &\equiv u(x, y, t) f(z) \\ v(x, y, z, t) &= v(x, y, t) f(z) \end{aligned}\right\} \tag{9}$$

with $f(z) \equiv$ constant if the bounding surfaces are free-slip; $f(z)$ would vanish at each wall and be parabolic (simulating Poiseuille flow) if the surfaces were no slip. Other possible forms for $f(z)$ would include a semiparabolic form for a combination of no-slip and free-slip, and a law-of-the-wall form for turbulent flows. In this last case, however, the addition of Reynolds stress terms would also be required.

It is convenient to let $f(z) \equiv 1.0$ on some surface, which may lie between the bounding surfaces or coincide with one of them; on this surface $u(x, y)$ and $v(x, y)$ are the actual horizontal velocity components. Let

$$\left.\begin{aligned} r(x, y) &\equiv \int_a^b f(z)\,dz, \\ s(x, y) &\equiv \int_a^b f^2(z)\,dz. \end{aligned}\right\} \tag{10}$$

Accordingly, the required equations become

$$\frac{\partial ru}{\partial x} + \frac{\partial rv}{\partial y} = 0, \tag{11}$$

$$\frac{\partial ru}{\partial t} + \frac{\partial su^2}{\partial x} + \frac{\partial suv}{\partial y} = -(b-a)\frac{\partial \phi}{\partial x} + \nu\left(\frac{\partial}{\partial x} r \frac{\partial u}{\partial x} + \frac{\partial}{\partial y} r \frac{\partial u}{\partial y}\right) + \nu u[f'(b) - f'(a)], \tag{12}$$

$$\frac{\partial rv}{\partial t} + \frac{\partial suv}{\partial x} + \frac{\partial sv^2}{\partial y} = -(b-a)\frac{\partial \phi}{\partial y} + \nu\left(\frac{\partial}{\partial x} r \frac{\partial v}{\partial x} + \frac{\partial}{\partial y} r \frac{\partial v}{\partial y}\right) + \nu v[f'(b) - f'(a)]. \tag{13}$$

It has been assumed that ϕ is independent of z, in analogy to the usual boundary-layer assumption, and the diffusion term has been modeled in a simple manner. The equations are now complete, the effects of the top and bottom walls being manifested in the variations of r and in the "friction" forces exerted by these surfaces.

Alternatively, if each bounding surface were moving parallel to itself, not changing shape, an appropriate form for the velocities, in place of Eq. (9), would be

$$u(x, y, z, t) = u(x, y, t) f(z) + \frac{(z-a)\, u_w(b) + (b-z)\, u_w(a)}{b-a}, \tag{14}$$

$$v(x, y, z, t) = v(x, y, t) f(z) + \frac{(z-a)\, v_w(b) + (b-z)\, v_w(a)}{b-a}, \tag{15}$$

where u_w and v_w are the prescribed wall velocities, and again $f(z)$ vanishes at each wall. This form assumes that the complete flow is superimposed over a simple linear (Couette) velocity profile. With this, Eq. (11) remains the same, whereas Eqs. (12) and (13) become somewhat more complicated in appearance, although no more so insofar as the numerical solution is concerned.

Differential Equations, Variable Wall Configuration

A very similar set of equations arises if the walls are allowed to move non-parallel to itself. We examine the symmetric case, which the plane $z = 0$ lies between two bounding surfaces, the motions of which mirror each other. Along $z = 0$, $w \equiv 0$, while along the upper surface, where $z = b(x, y, t)$,

$$w = \frac{\partial b}{\partial t} + u\frac{\partial b}{\partial x} + v\frac{\partial b}{\partial y}. \tag{16}$$

Integration of Eq. (1) gives

$$\frac{\partial b}{\partial t} + \frac{\partial}{\partial x}\int_0^b u\,dz + \frac{\partial}{\partial y}\int_0^b v\,dz = 0. \tag{17}$$

Integration of Eqs. (2) and (3) result in exactly the same equations as Eqs. (7) and (8), in which we put $a \equiv 0$, and $(\partial u/\partial z)_a \equiv (\partial v/\partial z)_a \equiv 0$. Thus, the principal effect of the moving wall appears to be manifested in Eq. (17). This is actually so if the wall is free slip, in which case we use Eq. (10) with $f(z) \equiv 1.0$ and obtain

$$\frac{\partial b}{\partial t} + \frac{\partial bu}{\partial x} + \frac{\partial bv}{\partial y} = 0, \tag{18}$$

$$\frac{\partial bu}{\partial t} + \frac{\partial bu^2}{\partial x} + \frac{\partial buv}{\partial y} = -b\frac{\partial \phi}{\partial x} + b\nu\left(\frac{\partial^2 u}{\partial x^2} + \frac{\partial^2 u}{\partial y^2}\right), \tag{19}$$

$$\frac{\partial bv}{\partial t} + \frac{\partial buv}{\partial x} + \frac{\partial bv^2}{\partial y} = -b\frac{\partial \phi}{\partial y} + b\nu\left(\frac{\partial^2 v}{\partial x^2} + \frac{\partial^2 v}{\partial y^2}\right). \tag{20}$$

It is apparent that b is closely analogous to the density function for compressible flow, in this case, however, being prescribed as a function of position and time so that the three equations for ϕ, u, and v are complete.

For a no-slip wall, $f(z)$ would be parabolic and must vanish at the variable wall position, so that r and s are functions of time, as well as position. It also becomes important to distinguish whether each element of the bounding wall moves only in the z-direction, or whether it also moves in the horizontal plane. Each example requires special treatment of the equations, but the principals of the numerical solution remain the same, as illustrated in the following Section.

Numerical Solution of the Equations

To illustrate the solution technique, we consider the case described by Eqs. (10)–(13). Since the procedure so closely resembles that of the usual SMAC technique [1], we simply outline the novel aspects as follows. First, we observe that the equation for transport of the quantity

$$Q \equiv \frac{\partial}{\partial y}\left(\frac{ru}{b-a}\right) - \frac{\partial}{\partial x}\left(\frac{rv}{b-a}\right)$$

is independent of the pressure. For this reason, a finite-difference time-advancement cycle utilizing an arbitrary field of ϕ values will nevertheless result in the correct value of Q everywhere except on the lateral boundaries of the flow field. In particular, with $\phi \equiv 0$, we may calculate tentative time-advanced velocities, $\tilde{u}_{i+1/2,j}$ and

$\tilde{v}_{i,j+1/2}$, which, while not correct, implant into the mesh the correct value at all interior mesh points of the quantity (which is analogous to vorticity):

$$Q_{i+1/2,j+1/2} \equiv \frac{1}{\delta y}\left[\left(\frac{ru}{b-a}\right)_{i+1/2,j+1} - \left(\frac{ru}{b-a}\right)_{i+1/2,j}\right] + \frac{1}{\delta x}\left[\left(\frac{rv}{b-a}\right)_{i+1,j+1/2} - \left(\frac{rv}{b-a}\right)_{i,j+1/2}\right]. \tag{21}$$

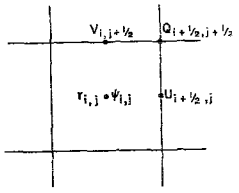

FIG. 1. Field variables locations in computational cell.

The indices label cell positions as shown in Fig. 1. The full equations for this part of the calculation are

$$\begin{aligned}\tilde{u}_{i+1/2,j} = u_{i+1/2,j} + \delta t \Bigg\{ & \frac{u_{i+1/2,j}}{r_{i+1/2,j}\,\delta x}\left(s_{i,j}u_{i-1/2,j} - s_{i+1,j}u_{i+3/2,j}\right) \\ & + \frac{1}{r_{i+1/2,j}\,\delta y}\left[(suv)_{i+1/2,j-1/2} - (suv)_{i+1/2,j+1/2}\right] \\ & + \frac{\nu}{r_{i+1/2,j}}\frac{1}{\delta x^2}\left\{r_{i+1,j}(u_{i+3/2,j} - u_{i+1/2,j}) - r_{i,j}(u_{i+1/2,j} - u_{i-1/2,j})\right\} \\ & + \frac{\nu}{r_{i+1/2,j}}\frac{1}{\delta y^2}\left\{r_{i+1/2,j+1/2}(u_{i+1/2,j+1} - u_{i+1/2,j})\right. \\ & \left. - r_{i+1/2,j-1/2}(u_{i+1/2,j} - u_{i+1/2,j-1})\right\} + \alpha_{i+1/2,j}\nu u_{i+1/2,j}\Bigg\},\end{aligned} \tag{22}$$

$$\begin{aligned}\tilde{v}_{i,j+1/2} = v_{i,j+1/2} + \delta t \Bigg\{ & \frac{1}{r_{i,j+1/2}\,\delta x}\left[(suv)_{i-1/2,j+1/2} - (suv)_{i+1/2,j+1/2}\right] \\ & - \frac{v_{i,j+1/2}}{\delta y}\left(s_{i,j}v_{i,j-1/2} - s_{i,j+1}v_{i,j+3/2}\right) \\ & + \frac{\nu}{r_{i,j+1/2}}\frac{1}{\delta x^2}\left\{r_{i+1/2,j+1/2}(v_{i+1,j+1/2} - v_{i,j+1/2})\right. \\ & \left. - r_{i-1/2,j+1/2}(v_{i,j+1/2} - v_{i-1,j+1/2})\right\} \\ & + \frac{\nu}{r_{i,j+1/2}}\frac{1}{\delta y^2}\left\{r_{i,j+1}(v_{i,j+3/2} - v_{i,j+1/2}) - r_{i,j}(v_{i,j+1/2} - v_{i,j-1/2})\right\} \\ & + \alpha_{i,j+1/2}\nu v_{i,j+1/2}\Bigg\}.\end{aligned} \tag{23}$$

The friction coefficient, α, is given by the expression $\alpha \equiv f'(b) - f'(a)$, describing the velocity shear gradients at the bounding walls.

Once the values of $\tilde{u}$ and $\tilde{v}$ have been determined, the problem is to find the final, correct velocities in such a way as to preserve the value of Q at every interior point, and simultaneously to satisfy the finite difference approximation to Eq. (10), namely

$$D_{i,j} \equiv \frac{1}{\delta x}[(ru)_{i+1/2,j} - (ru)_{i-1/2,j}] + \frac{1}{\delta y}[(rv)_{i,j+1/2} - (rv)_{i,j-1/2}] = 0. \tag{24}$$

To accomplish this, we introduce a potential function, $\psi_{i,j}$, such that

$$\frac{r_{i+1/2,j}(u^{\text{final}}_{i+1/2,j} - \tilde{u}_{i+1/2,j})}{(b-a)_{i+1/2,j}} = -\frac{\psi_{i+1,j} - \psi_{i,j}}{\delta x} \tag{25}$$

$$\frac{r_{i,j+1/2}(v^{\text{final}}_{i,j+1/2} + \tilde{v}_{i,j+1/2})}{(b-a)_{i,j+1/2}} = -\frac{\psi_{i,j+1} - \psi_{i,j}}{\delta y}. \tag{26}$$

Insertion of this into Eq. (21) shows that $Q^{\text{final}}_{i+1/2,j+1/2} \equiv \tilde{Q}_{i+1/2,j+1/2}$, as required. If $\tilde{D}_{ij}$ is calculated using the definition in Eq. (24), with the $\tilde{u}$, $\tilde{v}$ velocities, the result will generally not be zero. The goal is to achieve $D^{\text{final}}_{ij} = 0$, and accordingly we put Eqs. (25) and (26) into Eq. (24) to get an equation for determining ψ_{ij}:

$$\frac{1}{\delta x^2}[(b-a)_{i+1/2,j}(\psi_{i+1,j} - \psi_{i,j}) - (b-a)_{i-1/2,j}(\psi_{i,j} - \psi_{i-1,j})]$$
$$+ \frac{1}{\delta y^2}[(b-a)_{i,j+1/2}(\psi_{i,j+1} - \psi_{i,j}) - (b-a)_{i,j-1/2}(\psi_{i,j} - \psi_{i,j-1})] = \tilde{D}_{ij}. \tag{27}$$

Once this equation has been solved for ψ_{ij}, using either a direct-solution technique or an iterative procedure, the results can be used in Eqs. (25) and (26) to find the final velocities.

Nothing in this derivation precludes the possibility of having lateral boundaries in the form of rigid walls, input sources, continuative outputs, or free surfaces. The boundary conditions for these are direct extensions of those that have been discussed in detail in [1].

Internal Obstacles in Two-Dimensional Flows

While the SMAC method readily allows arbitrary placement of internal obstacles in two-dimensional flows, field variables stored for obstacle cells that have two or more adjacent nonobstacle cells must necessarily be multiple-valued. While this presents no conceptual difficulties, it usually results in computational time being spent on testing and additional bookkeeping chores.

The present SMAC extension may be used for the computation of two-dimensional flows with arbitrarily placed internal obstacles with none of the above difficulties. The flow field may be reduced to two-dimensional by setting $f(z) \equiv 1$ and using

$$r(x, y) = s(x, y) = b(x, y) - a(x, y) \text{ to define the obstacle.}$$

A flow without obstacles, for example, would have,

$$r(x, y) = b(x, y) - a(x, y) = r_0 \text{, a constant.}$$

Obstacle cells are defined by having r values of $-r_0$. Thus, an obstacle cell with an r value of $-r_0$ will have, on the cell boundary adjacent to a full cell, an r value of zero. This insures that no quantity is fluxed through that cell boundary, and cell-wise quantities stored for the obstacle cell do not effect the calculation. This may easily be illustrated by considering, for example, the ψ, Eq. (27). Let an obstacle be located at $i + 1, j$; see Fig. 2. The value of ψ_{ij} is obtained from the D_{ij} equation.

$$\frac{1}{\delta x^2}\left[r_{i+1/2,j}(\psi_{i+1,j} - \psi_{i,j}) - r_{i-1/2,j}(\psi_{i,j} - \psi_{i-1,j})\right]$$
$$+ \frac{1}{\delta y^2}\left[r_{i,j+1/2}(\psi_{i,j+1} - \psi_{i,j}) - r_{i,j-1/2}(\psi_{i,j} - \psi_{i,j-1})\right] = \tilde{D}_{ij} .$$

We can see that information coming out of the obstacle cell (in this case $\psi_{i+1,j}$) is multiplied by $r_{i+1/2,j} = 0$ so that it does not matter what value is stored for the potential function in the obstacle cell. Likewise, $\psi_{i+1,j}$ in the obstacle cell is independent of ψ's in the neighboring fluid cells. Thus, obstacle cells are completely uncoupled from the fluid region, meaning that all cells can be treated equally without special tests to enforce the desired boundary conditions. Of course, the velocity on any cell boundary having $r = 0$ must be maintained at zero.

Calculational Examples

The calculations for the following examples were all performed on the CDC 6600 computer. Results are presented in the form of cell centered velocity vector

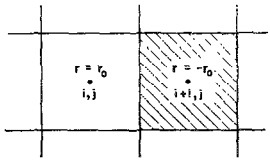

FIG. 2. Obstacle cell treatment for two-dimensional flows.

plots that were processed directly from the computer output on a Stromberg–Carlson 4020 Microfilm Recorder. The plots have been retouched only to show the location of the internal obstacle. In both examples, the fluid is viewed looking down the z axis at the x—y plane. For simplicity, both examples were calculated using $f(z) = 1$.

While the results were examined qualitatively to insure they are reasonable and stable, no quantitative comparisons with experiments were made.

The first example shows the flow over an underwater pyramid (Fig. 3) between two flat plates. The calculation was performed with the pyramid stationary and a prescribed velocity at the left boundary and continuative outflow at the right. The continuative boundary condition was obtained by having boundary cells to right of the last column of computational cells. The $\tilde{v}$ velocity of each boundary cell $(i + 1, j)$ was set equal to the corresponding $\tilde{v}$ velocity in the computational cell to the left (i, j), while the $\tilde{u}$ velocity for the last computational cell (i, j) was set equal to the $\tilde{u}$ velocity in the next to the last computational cell $(i - 1, j)$. The boundary conditions at $z = a$ and $z = b$ were free-slip.

The velocity vector plots shown in Fig. 4 have been transformed by subtracting the input velocity so that the pyramid appears to be moving to the left through a stationary fluid. The Reynolds number based upon the obstacle width at the top, the obstacle velocity, and the fluid viscosity is 150.

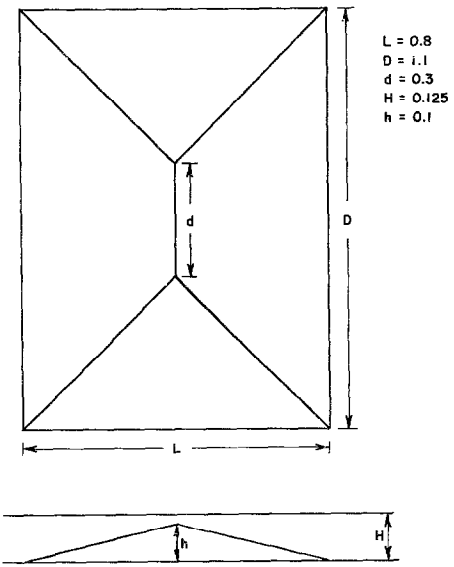

FIG. 3. Underwater pyramid for problem shown in Fig. 4.

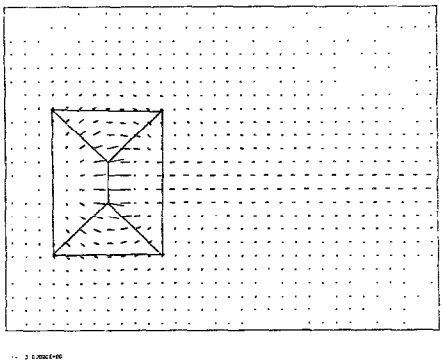

FIG. 4. Flow past underwater obstacle.

The fluid directly behind the pyramid is being sucked along while fluid also spills over the top and around the sides resulting in a stagnation area across the back of the pyramid. This example illustrates that even for the severe case where $h/H = 0.8$ (see Fig. 3) the calculation proceeds stably and gives qualitatively reasonable results.

To what extent the results are quantitatively accurate depends on the importance of the three-dimensional effects. It is apparent from the derivation of the approximate equations, (11–13), that there will be limitations imposed by the introduction of the f function. As three-dimensional effects become more important the choice of f will influence the accuracy of the results. Also, making the similarity assumption (Eq. 9) requires that

$$\frac{\partial(b-a)}{\partial x} \quad \text{and} \quad \frac{\partial(b-a)}{\partial y} \quad \text{be small.}$$

The above comments do not apply to the case of obstacles in two-dimensional flows since we are no longer trying to approximate three-dimensional effects.

The second example (Fig. 5) illustrates a two-dimensional flow with an internal

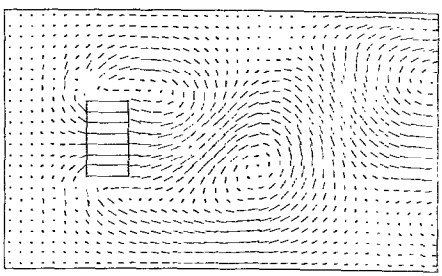

FIG. 5. Flow past two-dimensional obstacle.

obstacle. The boundary conditions on the sides of the obstacle are free-slip. The Reynolds number based on the obstacle width across the flow is 160 and the ratio of width to the distance between the plates is 1/3. The calculation was performed with the obstacle stationary and prescribed input and continuative output boundaries on the left and right respectively. The results, however, are again presented with the velocity vectors transformed by subtracting the input velocity so that the obstacle appears to be moving to the left while the fluid is at rest. The fluid behind the obstacle forms a vortex street that is confined by the top and bottom plates. A small amount of raggedness appears at the top of the vortex leaving the computing area at the upper right. These perturbations were generated at the front face of the obstacle when the problem was started impulsively and could probably have been eliminated if a smaller δt had been used for the first few computing cycles. However the perturbations remained bounded and were smoothly swept out of the continuative boundary. Subsequent vortices do not show this raggedness, as can be seen.

Acknowledgment

The authors would like to thank F. H. Harlow for initiating this study and who provided continual guidance and support.

Reference

1. A. A. Amsden and F. H. Harlow, A simplified MAC technique for incompressible fluid flow calculations, *J. Computational Phys.* **6** (1970), 322 and The SMAC Method: "A Numerical Technique for Calculating Incompressible Fluid Flows," Los Alamos Scientific Laboratory Report No. LA-4370, Los Alamos, N.M., 1970.